

# Geophysical Research Letters®



## RESEARCH LETTER

10.1029/2024GL109534

## The Influence of Non-Thermal Collisions in Europa's Atmosphere

Shane R. Carberry Mogan<sup>1</sup> , Andrew R. Poppe<sup>1</sup> , and Lucas Liuzzo<sup>1</sup> 

<sup>1</sup>Space Sciences Laboratory, University of California, Berkeley, CA, USA

### Key Points:

- DSMC modeling demonstrates that collisions cannot be neglected in modeling or analysis studies of Europa's atmosphere
- Collisions between radiolytically produced O<sub>2</sub> and its dissociated product O produce a non-thermal O<sub>2</sub> population and enhances O<sub>2</sub> escape
- The O<sub>2</sub> non-thermal densities and escape rates produced via O + O<sub>2</sub> collisions can far exceed those due to sputtering

### Supporting Information:

Supporting Information may be found in the online version of this article.

### Correspondence to:

S. R. Carberry Mogan,  
carberrymorgan@berkeley.edu

### Citation:

Carberry Mogan, S. R., Poppe, A. R., & Liuzzo, L. (2024). The influence of non-Thermal collisions in Europa's atmosphere. *Geophysical Research Letters*, 51, e2024GL109534. <https://doi.org/10.1029/2024GL109534>

Received 3 APR 2024

Accepted 22 SEP 2024

### Author Contributions:

**Formal analysis:** Andrew R. Poppe,

Lucas Liuzzo

**Funding acquisition:** Andrew R. Poppe,

Lucas Liuzzo

**Investigation:** Andrew R. Poppe,

Lucas Liuzzo

**Project administration:** Andrew

R. Poppe, Lucas Liuzzo

**Supervision:** Andrew R. Poppe,

Lucas Liuzzo

**Writing – review & editing:** Andrew

R. Poppe, Lucas Liuzzo

**Abstract** In this study, we show that non-thermal collisions can play a significant role in shaping Europa's exospheric structure. Collisions between radiolytically produced O<sub>2</sub> and the O produced via electron impact dissociation of O<sub>2</sub> affect the exospheric structure and escape rates. Specifically, O + O<sub>2</sub> collisions lead to the production of a non-thermal O<sub>2</sub> population, and increase the O<sub>2</sub> escape while decreasing the O escape. These collisions are dependent on three specific physical parameters: (a) the density of O<sub>2</sub>, (b) the electron impact dissociation rate of O<sub>2</sub>, and (c) the O + O<sub>2</sub> collision cross section. We demonstrate here that O + O<sub>2</sub> collisions affect Europa's atmosphere even in the lowest limits considered. Thus, to more accurately determine the influence O + O<sub>2</sub> collisions have on Europa's atmosphere in preparation for the forthcoming spacecraft missions, Europa Clipper and the JUPITER ICy moons Explorer (JUICE), these physical parameters need to be better constrained.

**Plain Language Summary** This study investigates the effects of collisions in Europa's atmosphere, specifically focusing on those involving oxygen atoms (O) and molecules (O<sub>2</sub>). We find that collisions between O<sub>2</sub> produced within Europa's icy surface and the O it produces via dissociative processes while aloft in the atmosphere can affect the structure of Europa's atmosphere as well as the rates at which neutral particles escape to the local space environment. The study highlights three important factors that influence these collisions: the density of O<sub>2</sub> near Europa's surface, how often O<sub>2</sub> molecules are broken apart by electrons producing O, and the size of the O + O<sub>2</sub> collision cross section. Constraining these values is crucial for accurately modeling Europa's atmosphere in preparation for the forthcoming spacecraft missions, Europa Clipper and the JUPITER ICy moons Explorer (JUICE).

## 1. Introduction

As the icy Galilean satellites of Jupiter—Europa, Ganymede, and Callisto—are continuously overtaken and bombarded by the charged particles within the Jovian magnetosphere, the spatially and temporally varying precipitation of the incident magnetospheric plasma onto their icy surfaces and atmospheres lead to a myriad of complex processes. Neutral atoms (H, O) and molecules (H<sub>2</sub>O, H<sub>2</sub>, OH) are directly sputtered from these icy surfaces, while other molecules (O<sub>2</sub>, H<sub>2</sub>) are produced via radiolysis in the ice from which they subsequently release (e.g., Johnson, 1990). The predominant radiolytic products in these atmospheres are molecular hydrogen and oxygen, where the former is primarily produced in a 2:1 stoichiometric ratio with the latter. Upon releasing from these icy surfaces, both molecular species accumulate in the atmospheres due to the infrequency of reactions occurring therein as well as the relatively low escape rates therefrom. Although O<sub>2</sub> and H<sub>2</sub> are expected to be the predominant species in these atmospheres near and far from the surfaces (e.g., Carberry Mogan et al., 2022; Marconi, 2007; Smyth & Marconi, 2006), respectively, only emissions from their dissociated products H and O have actually been detected in the gas-phase (e.g., Hall et al., 1995, 1998, Cunningham et al., 2015, Roth et al., 2016, 2017a, 2017b, Roth, 2021, Roth et al., 2021). Although these atoms can be produced directly via sputtering of ice (e.g., Bar-Nun et al. (1985); Kimmel and Orlando (1995)), they are primarily produced via dissociative processes of their parent molecules in the atmosphere (e.g., Vorburger et al., 2024).

Numerical models have been extensively applied to the icy Galilean satellites' atmospheres over the years to characterize and predict key aspects therein. At Callisto, it has been established that collisions must be considered in its atmosphere, for example, via molecular kinetics (MK) models (Carberry Mogan et al., 2020, 2021b, 2021a, 2022). At Ganymede, there is not yet a consensus on whether models of its atmosphere should include collisions (e.g., Leblanc et al., 2017; Marconi, 2007; Waite et al., 2024) or neglect them (e.g., Leblanc et al., 2023; Turc et al., 2014; Vorburger et al., 2022, 2024). However, if a study were carried out focusing on the influence of non-thermal collisions in Ganymede's atmosphere, such as that for H<sub>2</sub>+H collisions in Callisto's atmosphere (Carberry

© 2024. The Author(s).

This is an open access article under the terms of the [Creative Commons Attribution License](https://creativecommons.org/licenses/by/4.0/), which permits use, distribution and reproduction in any medium, provided the original work is properly cited.

Mogan et al., 2022) or the work presented here for O<sub>2</sub>+O collisions in Europa's atmosphere, a similar conclusion is likely: they should be considered.

At Europa, the topic of this study, collisions were considered in models of the atmosphere pre-2006 (Saur et al., 1998; Shematovich, 2006; Shematovich et al., 2005; Shematovich & Johnson, 2001; Smyth & Marconi, 2006), but more recent models have since neglected them (Cassidy et al., 2007; Oza et al., 2019; Plainaki et al., 2010, 2012, 2013; Teolis et al., 2017; Vorbürger & Wurz, 2018). Including collisions would not significantly affect the results presented in some of these studies (Cassidy et al., 2007; Oza et al., 2019) which focused on reproducing observed atmospheric asymmetries (McGrath et al., 2004; Roth et al., 2016) as a result of surface interactions. However, collisionless models in other studies were implemented under the assumption that if the atmosphere is too thin for O<sub>2</sub> molecules to frequently collide with one another, then collisions between *all* species can be neglected when modeling Europa's atmosphere (Plainaki et al., 2010, 2012, 2013; Vorbürger & Wurz, 2018), which other models have since used for their own justification (Lucchetti et al., 2016; Teolis et al., 2017). Here we demonstrate that, under closer scrutiny, this assumption does not hold. Indeed, if the same calculations used to justify a collisionless model according to Europa's O<sub>2</sub> component were applied to other atmospheric species, such as the O produced via electron impact dissociation of O<sub>2</sub>, they would indicate that collisions occur (see Supplementary Material in Supporting Information S1).

We simulate collisions in Europa's atmosphere using a MK model with inputs for its O<sub>2</sub>, H<sub>2</sub>, O, and H components consistent with values suggested in the literature. As will be seen, it is the *non-thermal* collisions, particularly those between radiolytically produced O<sub>2</sub> and the hot O (~eV) primarily produced via electron impact dissociation of O<sub>2</sub>, that have a significant effect on escape rates and the structure of Europa's atmosphere. Although the extent to which these collisions affect atmospheric escape and structure varies as a function of modeling inputs (e.g., surface densities, collision cross sections, and electron impact reaction rates), we demonstrate here that these collisions are non-negligible even in the lowest limits of the parameter space explored (i.e., the smallest collision cross section and lowest surface densities and electron impact reaction rates considered). Thus, collisions should be taken into account when modeling Europa's atmosphere.

Note that we are not attempting to provide a comprehensive model of Europa's atmosphere. Instead, our aim is to isolate the influence non-thermal collisions can have in Europa's atmosphere, and thus neglect other non-thermal sources, such as sputtering and interactions with the ionosphere (e.g., Dols et al., 2016). Future work will look to provide a more comprehensive model by including (and comparing) the influences of these processes.

## 2. Method

### 2.1. Molecular Kinetics Model

To simulate Europa's atmosphere and the influence of collisions therein we implement the direct simulation Monte Carlo (DSMC) method (Bird, 1994). The DSMC method is a molecular kinetics model which simulates macroscopic gas dynamics via stochastic microscopic processes using computational particles, each representing many real atoms (O and H) or molecules (O<sub>2</sub> and H<sub>2</sub>). The model implemented here was initially developed to simulate Callisto's tenuous atmosphere (Carberry Mogan et al., 2020, 2021b, 2021a, 2022), and has been adapted here to simulate Europa's atmosphere.

A 1D spherically symmetric simulation domain is employed in which radial cells span from Europa's surface,  $r_0 = R_E = 1560.8$  km, to its Hill sphere,  $r_{HS} \approx 8.7R_E$ . If a particle's trajectory crosses either of these boundaries, they are removed from the simulation and loss rates are calculated accordingly (see Supplementary Material in Supporting Information S1). This network of cells allows for particles to be locally grouped based on their position to simulate collisions as well as to take samples and calculate averages of the macroscopic flow. For further details on this DSMC model, we refer the reader to our earlier publications (e.g., Carberry Mogan et al., 2022) and the Supplemental Material in Supporting Information S1. We note that although our 1D model is inherently incapable of capturing local asymmetries in Europa's atmosphere (e.g., Oza et al., 2019), but neglecting such features do not affect the principal conclusions of this study.

## 2.2. Model Uncertainties

### 2.2.1. Surface Densities of O<sub>2</sub> and H<sub>2</sub>

For O<sub>2</sub> and H<sub>2</sub>, we implement steady-state thermal outgassing fluxes (see Supplementary Material in Supporting Information S1) calculated as a function of a prescribed surface density,  $n_0$ , which we vary over three orders of magnitude:  $n_{0,O_2} = 10^7 \text{ cm}^{-3}$ ,  $10^8 \text{ cm}^{-3}$ , and  $10^9 \text{ cm}^{-3}$ ;  $n_{0,H_2} = 10^5 \text{ cm}^{-3}$ ,  $10^6 \text{ cm}^{-3}$ , and  $10^7 \text{ cm}^{-3}$ . These values for  $n_{0,O_2}$  (and the corresponding column densities) fall within the broad range of those suggested in the literature (e.g., Eviatar et al., 1985; Hall et al., 1995; Hall et al., 1998; Hansen et al., 2005; Ip et al., 1998; Johnson et al., 1982; Johnson et al., 1998; Kliore et al., 1997; Plainaki et al., 2012; Roth et al., 2016; Saur et al., 1998; Saur et al., 2011; Shematovich, 2006; Shematovich et al., 2005; Shematovich & Johnson, 2001; Teolis et al., 2017; Vorburget & Wurz, 2018). Similarly,  $n_{0,H_2} = 10^5 \text{ cm}^{-3}$  and  $10^6 \text{ cm}^{-3}$  fall within the much more limited range of those suggested in the literature (e.g., Smyth & Marconi, 2006; Szalay et al., 2024), with  $n_{0,H_2} = 10^7 \text{ cm}^{-3}$  presenting an upper-bound case.

### 2.2.2. Electron Impact Reaction Rates

While aloft in the atmosphere, these molecules are susceptible to electron impacts, resulting in dissociation and/or ionization (see Supplementary Material in Supporting Information S1). If nascent H or O atoms are produced via electron impact dissociation, representative particles are injected into the simulation domain and subsequently tracked. The range of frequencies (hereafter referred to as rates) for electron impact reactions implemented in this study are taken from a recent study which analyzed the local electron environment in Europa's orbit and wake during Juno flybys (Szalay et al., 2024) (see Supplementary Material in Supporting Information S1). Szalay et al. (2024) demonstrated that these reaction rates can vary significantly, in some instances over an order of magnitude (see Extended Table 3 in Szalay et al., 2024).

### 2.2.3. Collision Cross Sections

Often in molecular kinetics simulations the biggest uncertainties stem from the implemented collision cross sections,  $\sigma$ . Elastic collisions between O<sub>2</sub> and H<sub>2</sub> particles are simulated using the variable hard sphere model (Bird, 1994). Elastic collisions between the non-thermal O and H atoms and the O<sub>2</sub> and H<sub>2</sub> molecules are simulated using the model derived by Lewkow and Kharchenko (2014), "LK14." Unfortunately for the purposes of this study, O + O<sub>2</sub> collisions have not been studied as in-depth as other atom-molecule collisions, such as O + N<sub>2</sub> (Balakrishnan et al., 1998; Kumar et al., 2023), at the energies relevant to this study. Instead, this collision has been studied at energies far larger (0.5–5.0 keV) than those relevant to Europa's atmosphere (Schafer et al., 1987). In addition, since O and O<sub>2</sub> have low-lying electronic states, collisions between excited oxygen atoms and molecules have been studied in more detail (e.g., Miura et al., 2002; Pan et al., 2019).

The LK14 model used here to derive  $\sigma_{O+O_2}$  (red lines in Figure 1) was originally developed to simulate keV protons precipitating into Mars' upper atmosphere. Although the model was utilized for a different energy regime than the work presented here ( $\lesssim$ eV), the authors suggested  $\sigma$  can be scaled according to the masses of the colliding species as well as the collision energy.

In Figure 1 we compare  $\sigma_{O+O_2}$  implemented here to  $\sigma$  calculated for O and other diatomic molecules, N<sub>2</sub> (Balakrishnan et al., 1998; Kumar et al., 2023) and H<sub>2</sub> (Gacesa & Kharchenko, 2014). A recent calculation for  $\sigma_{O+N_2}$  has been provided by Kumar et al. (2023), "K23," which we mass-scale to  $\sigma_{O+O_2}$  (see Supplementary Material in Supporting Information S1). Below  $\sim$ 0.1 eV, the mass-scaled  $\sigma_{O+N_2}$  is  $\sim$ 10 $\times$  larger than  $\sigma_{O+O_2}$  derived via the LK14 model, and the former approaches the latter with increasing energy to within a factor of  $\sim$ 2 by  $\sim$ 5 eV. We also mass-scaled  $\sigma_{O+H_2}$  calculated by Gacesa and Kharchenko (2014), "G14," to  $\sigma_{O+O_2}$ , which is seen to be at least  $\sim$ 5 $\times$  smaller than  $\sigma_{O+O_2}$  derived via the LK14 model throughout the considered energy range, and the discrepancy grows with increasing COM energy.

In an earlier DSMC model of Europa's atmosphere, Shematovich (2006) directly substituted  $\sigma_{O+N_2}$  calculated by Balakrishnan et al. (1998), "B98," for  $\sigma_{O+O_2}$ , which is  $\sim$ 5 $\times$  larger than  $\sigma_{O+O_2}$  derived via the LK14 model. While Smyth and Marconi (2006) did not explicitly list the value they used for  $\sigma_{O+O_2}$ , insight can be gained from a subsequent work by one of the authors involved. Marconi (2007), "M07," implemented a 2D DSMC model to simulate Ganymede's atmosphere composed of the same species as that of Europa, and  $\sigma_{O+O_2}$  was calculated as an

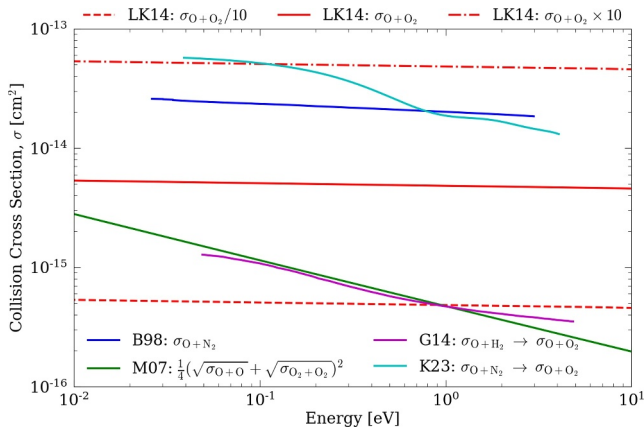


**Figure 1.** Collision cross sections,  $\sigma$ , implemented in this study for O + O<sub>2</sub> collisions (red lines) compared to similar  $\sigma$  derived in the literature. Balakrishnan et al. (1998), “B98” (blue), calculated  $\sigma_{\text{O}+\text{N}_2}$ ; Marconi (2007), “M07” (green) calculated  $\sigma_{\text{O}+\text{O}_2}$  as an average of  $\sigma_{\text{O}+\text{O}}$  and  $\sigma_{\text{O}_2+\text{O}_2}$ ; Gacesa and Kharchenko (2014), “G14” (magenta) calculated  $\sigma_{\text{O}+\text{H}_2}$ , which we mass-scaled to  $\sigma_{\text{O}+\text{O}_2}$ ; and Kumar et al. (2023), “K23” (cyan), calculated  $\sigma_{\text{O}+\text{N}_2}$ , which we mass-scaled to  $\sigma_{\text{O}+\text{O}_2}$ .

average of  $\sigma_{\text{O}+\text{O}}$  and  $\sigma_{\text{O}_2+\text{O}_2}$  derived elsewhere in the literature (see Table 3 and references therein). As can be seen, the resultant M07 distribution closely resembles the mass-scaled  $\sigma_{\text{O}+\text{H}_2}$ .

Thus, the  $\sigma_{\text{O}+\text{O}_2}$  we implement here lies somewhere in between that implemented in other DSMC models and the  $\sigma$  of O with other diatomic molecules. Therefore, to determine the influence of  $\sigma_{\text{O}+\text{O}_2}$  on our simulation results, we increased (dash-dotted red line in Figure 1) and decreased (dashed red line in Figure 1)  $\sigma_{\text{O}+\text{O}_2}$  derived via the LK14 model by a factor of 10 to more closely resemble these other  $\sigma$ . It should also be noted that the LK14 model has been used to simulate the same non-thermal collisions as those considered here in more recent DSMC models of the water-product atmospheres on Ganymede (Leblanc et al., 2017) and Callisto (Carberry Mogan et al., 2022). Thus, it is not without merit to apply the LK14 model to simulate non-thermal collisions in Europa’s atmosphere.

### 3. Results

#### 3.1. Non-Thermal Density Profiles

Figure 2 illustrates the density profiles for H<sub>2</sub>, O<sub>2</sub>, H, and O as a function of altitude for the prescribed surface densities,  $n_0$ , of O<sub>2</sub> ( $n_{0,\text{O}_2} = 10^7 \text{ cm}^{-3}$ ,  $10^8 \text{ cm}^{-3}$ , and  $10^9 \text{ cm}^{-3}$ ) with  $n_{0,\text{H}_2} = 10^5 \text{ cm}^{-3}$ . With increasing  $n_{0,\text{O}_2}$  the influence collisions have non-linearly increases compared to simulations which neglect such collisions. For example, with increasing  $n_{0,\text{O}_2}$  the production of hot O via electron impacts increases, but the initially hot O is more efficiently thermalized by collisions with a more dense O<sub>2</sub> component. As a result, the O density significantly increases relative to a simulation in which such collisions are neglected: with  $n_{0,\text{O}_2} = 10^7 \text{ cm}^{-3}$ , there is a negligible difference in O density when collisions are considered versus when they are neglected; with  $n_{0,\text{O}_2} = 10^8 \text{ cm}^{-3}$ , the O density effectively doubles within  $\sim 1,000 \text{ km}$  of the surface as a result of collisions with O<sub>2</sub>; and with  $n_{0,\text{O}_2} = 10^9 \text{ cm}^{-3}$ , the O density is enhanced by almost two orders of magnitude near the surface. As the hot O component thermalizes via O + O<sub>2</sub> collisions, the initially thermal O<sub>2</sub> component is heated; and a larger  $n_{0,\text{O}_2}$  results in more hot O being produced, which in turn inflates the non-thermal O<sub>2</sub> component due to more frequent O + O<sub>2</sub> collisions. Also with  $n_{0,\text{O}_2} = 10^9 \text{ cm}^{-3}$ , the densities of the H<sub>2</sub> and H components are diminished over the same altitude range in which the O densities are enhanced. This is due to the H<sub>2</sub> having to diffuse through a much denser O<sub>2</sub> component, which can knock more H<sub>2</sub> particles back down to the surface, which is treated as a sink in our steady-state model, thereby inhibiting their otherwise upward trajectories and reducing atmospheric escape (illustrated later in Figure 4). As a result, the density of the H produced by H<sub>2</sub> is also reduced.

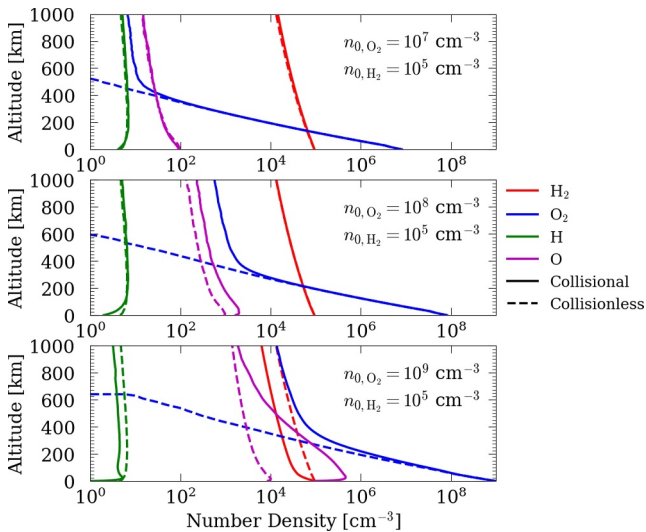


**Figure 2.** Density profiles for H<sub>2</sub> (red), O<sub>2</sub> (blue), H (green), and O (magenta) as a function of altitude for the prescribed surface densities,  $n_0$ , of O<sub>2</sub> (top:  $n_{0,\text{O}_2} = 10^7 \text{ cm}^{-3}$ , middle:  $n_{0,\text{O}_2} = 10^8 \text{ cm}^{-3}$ , and bottom:  $n_{0,\text{O}_2} = 10^9 \text{ cm}^{-3}$ ) with  $n_{0,\text{H}_2} = 10^5 \text{ cm}^{-3}$  in DSMC simulations which included (solid lines) and neglected (dashed lines) collisions.

#### 3.2. Influence of Model Uncertainties

In Figure 3, we show results from case studies where we fixed  $n_{0,\text{H}_2}$  and  $n_{0,\text{O}_2}$  at their respective median values,  $10^6 \text{ cm}^{-3}$  and  $10^8 \text{ cm}^{-3}$ , and varied  $\sigma_{\text{O}+\text{O}_2}$  and electron impact dissociation rates. When collisions are neglected, the resultant density profile is isothermal, whereby the density effectively drops off as a function of the local scale height,  $H \sim 25 \text{ km}$ , calculated according to the prescribed surface temperature,  $T_0 = 125 \text{ K}$ . When collisions are included, however, the O<sub>2</sub> component is heated via O + O<sub>2</sub> collisions, resulting in a sharp transition in  $H$ . Depending on the implemented electron impact dissociation rate ( $0.56\text{--}5.6 \times 10^{-6} \text{ s}^{-1}$ ) and  $\sigma_{\text{O}+\text{O}_2}$  (Figure 1), the altitude at which this transition occurs varies from  $\sim 100 \text{ km}$  to  $\sim 400 \text{ km}$  and the corresponding non-thermal O<sub>2</sub> density at an altitude of  $\sim 1,000 \text{ km}$  varies



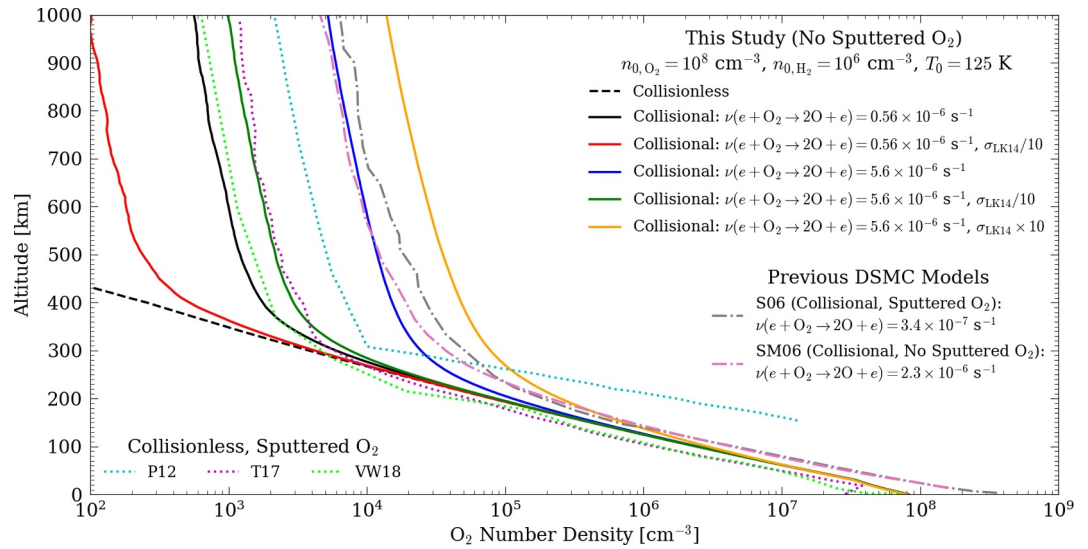


**Figure 3.** O<sub>2</sub> density profiles from DSMC simulations in which collisions were included (solid colored lines) and neglected (dashed black line), and the electron impact dissociation rate,  $\nu$ , and O + O<sub>2</sub> collision cross section,  $\sigma_{O+O_2}$ , were varied. Results are also compared to those of earlier DSMC models of Europa's atmosphere (dash-dotted lines; Shematovich, 2006, “S06,” gray, and Smyth & Marconi, 2006, “SM06,” pink) as well as collisionless models which included sputtering as the lone non-thermal source of O<sub>2</sub> (dotted lines; Plainaki et al., 2012, “P12,” cyan, Teolis et al., 2017, “T17,” magenta, and Vorburger & Wurz, 2018, “VW18,” lime green).

from  $\sim 10^4 \text{ cm}^{-3}$  to  $\sim 10^2 \text{ cm}^{-3}$ , respectively. When electron impact dissociation rates are kept the same but  $\sigma_{O+O_2}$  is reduced by a factor of 10, the altitude at which this transition occurs increases and, thus, the density of the non-thermal O<sub>2</sub> component decreases; that is, with a smaller  $\sigma_{O+O_2}$ , fewer O + O<sub>2</sub> collisions occur such that the O<sub>2</sub> component is heated less. However, even when implementing these relatively small  $\sigma_{O+O_2}$ , O + O<sub>2</sub> collisions can still significantly affect the O<sub>2</sub> density profile.

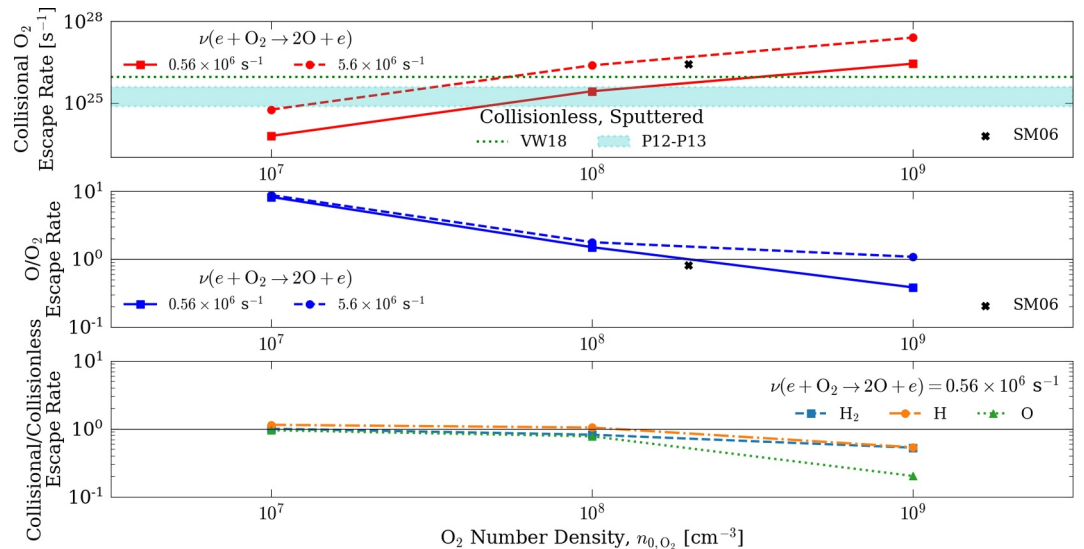


**Figure 4.** *Top:* O<sub>2</sub> escape rates induced via non-thermal collisions. Results are shown for a range of prescribed  $n_{O_2}$  (with  $n_{H_2}$  fixed to  $10^6 \text{ cm}^{-3}$ ) as well as electron impact dissociation rates,  $\nu$ , and are compared to those from Smyth and Marconi (2006), “SM06,” Plainaki et al. (2012, 2013), “P12-13,” and Vorburger and Wurz (2018), “VW18.” *Middle:* Ratio of escape between O and O<sub>2</sub> as a function of  $n_{O_2}$  and  $\nu$  and compared to that from SM06. *Bottom:* Ratio of escape rates between simulations with and without collisions for H<sub>2</sub> (dashed blue line), H (dash-dotted orange line), and O (dotted green line).

Interestingly, the radial profile of the non-thermal O<sub>2</sub> component produced via O + O<sub>2</sub> collisions resembles that of O<sub>2</sub> sputtered from the surface with a high-energy tail in exospheric models of Europa's atmosphere (e.g., Plainaki et al., 2012; Teolis et al., 2017; Vorbürger & Wurz, 2018). Depending on the electron impact dissociation rate and  $\sigma_{\text{O}+\text{O}_2}$ , however, these collisions can produce more non-thermal O<sub>2</sub> than can sputtering. The non-thermal O<sub>2</sub> component produced via O + O<sub>2</sub> collisions is also consistent with earlier DSMC models of Europa's atmosphere (Shematovich, 2006; Smyth & Marconi, 2006) which also included such collisions. In the upper limit case considered here, when the electron impact dissociation rate is  $5.6 \times 10^{-6} \text{ m}^{-1}$  and  $\sigma_{\text{O}+\text{O}_2}$  derived by the LK14 model is enhanced by a factor of 10, the non-thermal O<sub>2</sub> component produced is more dense than that of the models of Smyth and Marconi (2006) and Shematovich (2006) by  $\sim 150$  km despite their  $n_{\text{O},\text{O}_2}$  being larger.

The differences in results from our DSMC model to those of Smyth and Marconi (2006) and Shematovich (2006) are due to the different modeling inputs. Smyth and Marconi (2006) implemented a different electron impact reaction rate ( $2.6 \times 10^{-6} \text{ m}^{-1}$ ; c.f., Figure 3), initial speed of hot O (1.85 km/s; c.f., Supplementary Material in Supporting Information S1), and  $\sigma_{\text{O}+\text{O}_2}$  (see M07 in Figure 1) compared to those considered here. Shematovich (2006) included the high-energy tail for sputtered O<sub>2</sub>, a smaller electron impact dissociation rates ( $3.4 \times 10^{-7} \text{ m}^{-1}$ ; c.f., Figure 3), a different initial speed distribution of hot O produced via electron impacts (Cosby, 1993; c.f., Supplementary Material in Supporting Information S1), and a different  $\sigma_{\text{O}+\text{O}_2}$  (see B98 in Figure 1). Note Shematovich (2006) also considered photodissociation of O<sub>2</sub> and dissociative recombination of O<sub>2</sub><sup>+</sup> as additional sources for hot O, but we only compare our results to their model in which electron impact dissociation of O<sub>2</sub> was the sole source. Shematovich (2006) assumed a relatively small electron impact reaction rate, so that their assumed photodissociation rate ( $1.8 \times 10^{-7} \text{ m}^{-1}$ ; see Table 2 in Shematovich et al., 2005) produced a comparable amount of O. In contrast, we assumed electron impact dissociation rates  $\sim 2\text{--}20\times$  larger than Shematovich (2006)—and even larger rates are expected (Szalay et al., 2024). Shematovich (2006) also assumed a smaller excess energy for photodissociation than electron impact dissociation, so that the O produced via the former were more likely to thermalize via collisions with O<sub>2</sub> than the O produced via the latter. As a result, a  $\sim 1$  order of magnitude denser O component was produced when both of these sources were considered as opposed to only electron impact dissociation (see Figure 5 in Shematovich et al., 2005). Including photodissociation of O<sub>2</sub> in our models would have a negligible effect on our results. Furthermore, Shematovich (2006) also considered a case where dissociative recombination of O<sub>2</sub><sup>+</sup> was the sole source of O, but a negligible amount was produced compared to dissociation of neutral O<sub>2</sub>. Thus, we can safely neglect this non-thermal source of O as well.

### 3.3. Atmospheric Escape

Figure 4 illustrates the influence non-thermal collisions also have on neutral escape rates from Europa's atmosphere. Since we assume O<sub>2</sub> thermally desorbs from Europa's icy surface (see Supplementary Material in Supporting Information S1) and neglect the high-energy tail of the velocity distribution for sputtered O<sub>2</sub>, there is no O<sub>2</sub> escape when we neglect collisions. Thus, the only escape mechanism for O<sub>2</sub> considered here is due to collisions with hot H and O. Therefore, in the top panel of Figure 4 we plot the simulated O<sub>2</sub> escape rates only from the simulations in which collisions are considered. Increasing the electron impact dissociation rate causes an increase in the O<sub>2</sub> escape rate, as the production of more non-thermal O leads to a greater number of O + O<sub>2</sub> collisions (as well as a more dense non-thermal O<sub>2</sub> component, Figure 3).

We compare the range of simulated O<sub>2</sub> escape rates to that of Smyth and Marconi (2006), who also only simulated thermally desorbing O<sub>2</sub> so that the only escaping O<sub>2</sub> was due to non-thermal collisions. Although Smyth and Marconi (2006) implemented different modeling inputs (see Section 3.2), their simulated O<sub>2</sub> escape rates align nicely with those of this study within the range of electron impact dissociation rates considered. We also compare our simulated escape rates to those from models of Europa's atmosphere where sputtering of O<sub>2</sub> was considered but collisions were neglected (Plainaki et al., 2012, 2013; Vorbürger & Wurz, 2018). That is, in these collisionless models O<sub>2</sub> only escapes as a result of the high-energy tail of its initial velocity distribution. As can be seen, depending on  $n_{\text{O},\text{O}_2}$  and the electron impact dissociation rate, O + O<sub>2</sub> collisions can lead to significantly more O<sub>2</sub> escape than can sputtering.

In the simulations in which collisions are considered, we also examined the ratio of O escape to that of O<sub>2</sub> (middle panel of Figure 4). With  $n_{\text{O},\text{O}_2} = 10^7 \text{ cm}^{-3}$ , the ratio of O-to-O<sub>2</sub> escape is  $\sim 9$  regardless of the electron impact dissociation rate. This is consistent with the O density profile with and without collisions shown in Figure 2; that

is, with  $n_{0,O_2} = 10^7 \text{ cm}^{-3}$ , O + O<sub>2</sub> collisions do not noticeably affect the O component. However, for  $n_{0,O_2} \gtrsim 10^8 \text{ cm}^{-3}$ , a non-linear relationship between the simulated escape rates and these collisions is demonstrated as the O-to-O<sub>2</sub> escape ratios begin to significantly diverge from one another. When the electron impact dissociation rate is enhanced by a factor of 10, the O<sub>2</sub> escape is similarly enhanced (top panel in Figure 4). However, the same is not true for the escaping hot O: with  $n_{0,O_2} \gtrsim 10^9 \text{ cm}^{-3}$ , the ratio of O-to-O<sub>2</sub> escape with an electron impact dissociation rate of  $5.6 \times 10^{-6} \text{ s}^{-1}$  is  $\sim 3\times$  more than that with a rate of  $0.56 \times 10^{-6} \text{ s}^{-1}$  (O escapes 20 $\times$  more in the former simulation than in the latter). Moreover, with  $n_{0,O_2} \gtrsim 10^9 \text{ cm}^{-3}$  and an electron impact dissociation rate of  $0.56 \times 10^{-6} \text{ s}^{-1}$ , more O<sub>2</sub> escapes than O. Smyth and Marconi (2006) predicts slightly less atomic O escape than in our models, which, again, is likely a result of the difference in modeling inputs mentioned above. However, both Smyth and Marconi (2006) and our simulations with an electron impact dissociation rate of  $0.56 \times 10^{-6} \text{ s}^{-1}$  suggest that for  $n_{0,O_2} \gtrsim 3 \times 10^8 \text{ cm}^{-3}$  more oxygen will escape Europa's atmosphere in molecular form rather than atomic.

Finally, in the bottom panel of Figure 4 we compare the ratios of escape rates for the H<sub>2</sub>, H, and O components from simulations in which collisions are considered compared to when they are neglected across the range of  $n_{0,O_2}$  considered with  $n_{0,H_2} = 10^6 \text{ cm}^{-3}$ . For all three species, collisions with O<sub>2</sub> suppress escape compared to simulations without collisions, with O being the most affected; for example, with  $n_{0,O_2} = 10^9 \text{ cm}^{-3}$ , the O escape rate is reduced by  $\sim 5$ . Since we simulate H<sub>2</sub> thermally desorbing from the surface, one can analytically calculate the expected escape rates in a collisionless simulation via the Jeans formula according to  $n_0$  and  $T_0$  (e.g., Carberry Mogan et al., 2020). As can be seen, however, collisions with a much denser O<sub>2</sub> component result in *sub*-Jeans escape, making analytically estimating thermal H<sub>2</sub> escape more difficult.

#### 4. Conclusion

Here we have demonstrated that collisions can play a significant role in shaping Europa's exospheric structure. Non-thermal collisions between the O<sub>2</sub> component, the most dense species near the surface, and the hot O it produces via electron impact dissociation produces a significant non-thermal O<sub>2</sub> population and enhances O<sub>2</sub> escape. Comparing our simulation results to those of collisionless models in which sputtering is the lone non-thermal source of O<sub>2</sub> (Plainaki et al., 2012, 2013; Teolis et al., 2017; Vorbürger & Würz, 2018) suggests that larger non-thermal O<sub>2</sub> densities and escape rates can result from these collisions than from sputtering. This result complicates the idea often posited for surface bound exospheres produced as a result of magnetospheric plasma bombardment (Plainaki et al., 2018; Szalay et al., 2024): that if an otherwise thermal component of the atmosphere (e.g., O<sub>2</sub>) is detected at high altitudes, for example, by an in-situ spacecraft, then it was likely sputtered in order to obtain the energy required to reach such heights; and knowing that this detected species comes directly from the surface, these observations can be used to extrapolate information about the surface, such as source rates and composition. However, we have demonstrated that non-thermal O<sub>2</sub> can reach these same altitudes as a result of O + O<sub>2</sub> collisions, and as such, inferring information about the surface becomes more complicated.

Since previous collisionless models did not account for sputtered O<sub>2</sub> molecules depositing their energy within a collisional atmosphere, their simulated neutral O<sub>2</sub> escape rates due to sputtering should be considered as *upper limits*. In addition, we show that as the O<sub>2</sub> density increases, the escape rates of H<sub>2</sub>, H, and O decrease, again suggesting that the escape rates presented for these species by collisionless models should also be considered as upper limits. Thus, a model of Europa's atmosphere must take into account collisions *and* sputtering to determine the total atmospheric escape rates, from which surface composition and evolution can be inferred (e.g., Szalay et al., 2024) as well as the source rates for a neutral torus can be derived (e.g., Smith et al., 2019; Szalay et al., 2022).

Finally, the influence of non-thermal collisions in Europa's atmosphere are largely dependent on three key physical parameters: the surface density of O<sub>2</sub>, the electron impact dissociation rates which produce hot O, and the collision cross sections implemented to simulate O + O<sub>2</sub> collisions. Whereas the first two parameters implemented here are taken from established values in the literature, the O + O<sub>2</sub> collision cross section was roughly approximated using a scaling model from the literature. Although we varied the size of this collision cross section to resemble those in the literature for similar collisions, future work can improve on this treatment by deriving this collision cross section, for example, in a manner similar to recent studies which derived collision cross sections for hot O colliding with molecules present in other topical planetary atmospheres (e.g., Chhabra et al., 2023;

Gacesa et al., 2020; Kumar et al., 2023). Indeed, this collision has been shown here to be crucial in affecting the evolution of Europa's atmosphere, and likely has a similar influence on the O<sub>2</sub>-rich atmospheres of the other icy Galilean satellites, Ganymede and Callisto, all of which are soon to be the subject of upcoming spacecraft missions (Clipper and JUICE). Moreover, the influence of this collision will likely affect the interpretation of the Juno flyby of Europa from which O<sub>2</sub> production rates were inferred (Szalay et al., 2024): the pick-up ions detected by Juno suggested a highly non-thermal population in Europa's atmosphere; however, only atmospheric and direct surface sputtering and/or Joule heating were considered as a possible heating mechanism, and not non-thermal collisions like those presented here.

## Data Availability Statement

Results used in this study can be found in Carberry Mogan et al. (2024).

## Acknowledgments

The authors acknowledge support from NASA Solar System Workings Grants 80NSSC21K0152 and 80NSSC22K0097.

## References

- Balakrishnan, N., Kharchenko, V., & Dalgarno, A. (1998). Slowing of energetic O(<sup>3</sup>P) atoms in collisions with N<sub>2</sub>. *Journal of Geophysical Research*, 103(A10), 23393–23398. <https://doi.org/10.1029/98ja02198>
- Bar-Nun, A., Herman, G., Rappaport, M. L., & Mekler, Y. (1985). Ejection of H<sub>2</sub>O, O<sub>2</sub>, H<sub>2</sub> and H from water ice by 0.5–6 keV H<sup>+</sup> and Ne<sup>+</sup> ion bombardment. *Surface Science*, 150(1), 143–156. [https://doi.org/10.1016/0039-6028\(85\)90215-8](https://doi.org/10.1016/0039-6028(85)90215-8)
- Bird, G. A. (1994). Molecular gas dynamics and the direct simulation of gas flows.
- Carberry Mogan, S. R., Liuzzo, L., & Poppe, A. R. (2024). Data for “The influence of non-thermal collisions in Europa’s atmosphere” by Carberry Mogan et al. (2024). Available at <https://doi.org/10.5281/zenodo.10892311>
- Carberry Mogan, S. R., Tucker, O. J., & Johnson, R. E. (2021a). The influence of upper boundary conditions on molecular kinetic atmospheric escape simulations. *Planetary and Space Science*, 205, 105302. <https://doi.org/10.1016/j.pss.2021.105302>
- Carberry Mogan, S. R., Tucker, O. J., Johnson, R. E., Roth, L., Alday, J., Vorbuerger, V., et al. (2022). Callisto's atmosphere: First evidence for H<sub>2</sub> and constraints on H<sub>2</sub>O. *Journal of Geophysical Research: Planets*, 127(11). <https://doi.org/10.1029/2022je007294>
- Carberry Mogan, S. R., Tucker, O. J., Johnson, R. E., Sreenivasan, K. R., & Kumar, S. (2020). The influence of collisions and thermal escape in Callisto's atmosphere. *Icarus*, 352, 113932. <https://doi.org/10.1016/j.icarus.2020.113932>
- Carberry Mogan, S. R., Tucker, O. J., Johnson, R. E., Vorbuerger, A., Galli, A., Marchand, B., et al. (2021b). A tenuous, collisional atmosphere on Callisto. *Icarus*, 368, 114597. <https://doi.org/10.1016/j.icarus.2021.114597>
- Cassidy, T. A., Johnson, R. E., McGrath, M. A., Wong, M. C., & Cooper, J. F. (2007). The spatial morphology of Europa's near-surface O<sub>2</sub> atmosphere. *Icarus*, 191(2), 755–764. <https://doi.org/10.1016/j.icarus.2007.04.033>
- Chhabra, S., Gacesa, M., Khalil, M. S., Al Ghaferi, A., & El-Kork, N. (2023). A quantum-mechanical investigation of O(<sup>3</sup>P) + CO scattering cross sections at superthermal collision energies. *Monthly Notices of the Royal Astronomical Society*, 519(1), 1253–1260. <https://doi.org/10.1093/mnras/stac3057>
- Cosby, P. C. (1993). Electron-impact dissociation of oxygen. *The Journal of Chemical Physics*, 98(12), 9560–9569. <https://doi.org/10.1063/1.464387>
- Cunningham, N. J., Spencer, J. R., Feldman, P. D., Strobel, D. F., France, K., & Osterman, S. N. (2015). Detection of Callisto's oxygen atmosphere with the hubble space telescope. *Icarus*, 254, 178–189. <https://doi.org/10.1016/j.icarus.2015.03.021>
- Dols, V. J., Bagenal, F., Cassidy, T. A., Cray, F. J., & Delamere, P. A. (2016). Europa's atmospheric neutral escape: Importance of symmetrical O<sub>2</sub> charge exchange. *Icarus*, 264, 387–397. <https://doi.org/10.1016/j.icarus.2015.09.026>
- Eviatar, A., Bar-nun, A., & Podolak, M. (1985). European surface phenomena. *Icarus*, 61(2), 185–191. [https://doi.org/10.1016/0019-1035\(85\)90100-9](https://doi.org/10.1016/0019-1035(85)90100-9)
- Gacesa, M., & Kharchenko, V. (2014). Quantum reactive scattering of O(<sup>3</sup>P)+H<sub>2</sub> at collision energies up to 4.4 eV. *The Journal of Chemical Physics*, 141(16). <https://doi.org/10.1063/1.4899179>
- Gacesa, M., Lillis, R. J., & Zahnle, K. J. (2020). O(<sup>3</sup>P) + CO<sub>2</sub> scattering cross-sections at superthermal collision energies for planetary aeronomy. *Monthly Notices of the Royal Astronomical Society*, 491(4), 5650–5659. <https://doi.org/10.1093/mnras/stz3366>
- Hall, D. T., Feldman, P. D., McGrath, M. A., & Strobel, D. F. (1998). The far-ultraviolet oxygen airglow of Europa and Ganymede. *The Astrophysical Journal*, 499(1), 475–481. <https://doi.org/10.1086/305604>
- Hall, D. T., Strobel, D. F., Feldman, P. D., McGrath, M. A., & Weaver, H. A. (1995). Detection of an oxygen atmosphere on Jupiter's moon Europa. *Nature*, 373(6516), 677–679. <https://doi.org/10.1038/373677a0>
- Hansen, C. J., Shemansky, D. E., & Hendrix, A. R. (2005). Cassini UVIS observations of Europa's oxygen atmosphere and torus. *Icarus*, 176(2), 305–315. <https://doi.org/10.1016/j.icarus.2005.02.007>
- Ip, W.-H., Williams, D. J., McEntire, R. W., & Mauk, B. H. (1998). Ion sputtering and surface erosion at Europa. *Geophysical Research Letters*, 25(6), 829–832. <https://doi.org/10.1029/98gl00472>
- Johnson, R. E. (1990). *Energetic charged-particle interactions with atmospheres and surfaces*. Springer Science and Business Media.
- Johnson, R. E., Killen, R. M., Waite Jr, J. H., & Lewis, W. S. (1998). Europa's surface composition and sputter-produced ionosphere. *Geophysical Research Letters*, 25(17), 3257–3260. <https://doi.org/10.1029/98gl02565>
- Johnson, R. E., Lanzerotti, L. J., & Brown, W. L. (1982). Planetary applications of ion induced erosion of condensed-gas frosts. *Nuclear Instruments and Methods in Physics Research*, 198(1), 147–157. [https://doi.org/10.1016/0167-5087\(82\)90066-7](https://doi.org/10.1016/0167-5087(82)90066-7)
- Kimmel, G. A., & Orlando, T. M. (1995). Low-energy (5–120 eV) electron-stimulated dissociation of amorphous D<sub>2</sub>O ice: D(2S), O(3P<sub>2</sub>,1,0), and O(1D<sub>2</sub>) yields and velocity distributions. *Physical Review Letters*, 75(13), 2606.
- Kliore, A. J., Hinson, D. P., Flasar, F. M., Nagy, A. F., & Cravens, T. E. (1997). The ionosphere of Europa from Galileo radio occultations. *Science*, 277(5324), 355–358. <https://doi.org/10.1126/science.277.5324.355>
- Kumar, S., Kumar, S., Gacesa, M., El-Kork, N., & Yamijala, S. S. R. K. C. (2023). Quantum scattering cross-sections for O(<sup>3</sup>P) + N<sub>2</sub> collisions for planetary aeronomy. *Monthly Notices of the Royal Astronomical Society*, 526(4), 5675–5681. <https://doi.org/10.1093/mnras/stad3149>
- Leblanc, F., Oza, A. V., Leclercq, L., Schmidt, C., Cassidy, T., Modolo, R., et al. (2017). On the orbital variability of Ganymede's atmosphere. *Icarus*, 293, 185–198. <https://doi.org/10.1016/j.icarus.2017.04.025>



- Leblanc, F., Roth, L., Chaufray, J.-Y., Modolo, R., Galand, M., Ivchenko, N., et al. (2023). Ganymede's atmosphere as constrained by HST/STIS observations. *Icarus*, 399, 115557. <https://doi.org/10.1016/j.icarus.2023.115557>
- Lewkow, N. R., & Kharchenko, V. (2014). Precipitation of energetic neutral atoms and induced non-thermal escape fluxes from the Martian atmosphere. *The Astrophysical Journal*, 790(2), 98. <https://doi.org/10.1088/0004-637x/790/2/98>
- Lucchetti, A., Plainaki, C., Cremonese, G., Milillo, A., Cassidy, T. A., Jia, X., & Shematovich, V. (2016). Loss rates of Europa's tenuous atmosphere. *Planetary and Space Science*, 130, 14–23. <https://doi.org/10.1016/j.pss.2016.01.009>
- Marconi, M. L. (2007). A kinetic model of Ganymede's atmosphere. *Icarus*, 190(1), 155–174. <https://doi.org/10.1016/j.icarus.2007.02.016>
- McGrath, M. A., Lellouch, E., Strobel, D. F., Feldman, P. D., & Johnson, R. E. (2004). Satellite atmospheres. *Jupiter: The Planet, Satellites and Magnetosphere*, 457–483.
- Miura, N., Hashimoto, K., Takahashi, K., Taniguchi, N., & Matsumi, Y. (2002). Nobuaki Miura, Kenro Hashimoto, Kenshi Takahashi, Nori Taniguchi, Yutaka Matsumi; Electronic quenching of O(<sup>1</sup>D) by collisions with O<sub>2</sub>: A theoretical study in a collinear case. *The Journal of Chemical Physics*, 116(13), 5551–5556. <https://doi.org/10.1063/1.1457433>
- Oza, A. V., Leblanc, F., Johnson, R. E., Schmidt, C., Leclercq, L., Cassidy, T. A., & Chaufray, J.-Y. (2019). Dusk over dawn O<sub>2</sub> asymmetry in Europa's near-surface atmosphere. *Planetary and Space Science*, 167, 23–32. <https://doi.org/10.1016/j.pss.2019.01.006>
- Pan, T.-J., Wilson, T. J., & Stephani, K. A. (2019). Vibrational state-specific model for dissociation and recombination of the O<sub>2</sub> (<sup>3</sup>Σ<sub>g</sub><sup>-</sup>) + O (<sup>3</sup>P) system in DSMC. *The Journal of Chemical Physics*, 150(7). <https://doi.org/10.1063/1.5035283>
- Plainaki, C., Cassidy, T. A., Shematovich, V. I., Milillo, A., Wurz, P., Vorbürger, A., et al. (2018). Towards a global unified model of Europa's tenuous atmosphere. *Space Science Reviews*, 214(1), 1–71. <https://doi.org/10.1007/s11214-018-0469-6>
- Plainaki, C., Milillo, A., Mura, A., Orsini, S., & Cassidy, T. (2010). Neutral particle release from Europa's surface. *Icarus*, 210(1), 385–395. <https://doi.org/10.1016/j.icarus.2010.06.041>
- Plainaki, C., Milillo, A., Mura, A., Orsini, S., Massetti, S., & Cassidy, T. (2012). The role of sputtering and radiolysis in the generation of Europa exosphere. *Icarus*, 218(2), 956–966. <https://doi.org/10.1016/j.icarus.2012.01.023>
- Plainaki, C., Milillo, A., Mura, A., Saur, J., Orsini, S., & Massetti, S. (2013). Exospheric O<sub>2</sub> densities at Europa during different orbital phases. *Planetary and Space Science*, 88, 42–52. <https://doi.org/10.1016/j.pss.2013.08.011>
- Roth, L. (2021). A stable H<sub>2</sub>O atmosphere on Europa's trailing hemisphere from HST images. *Geophysical Research Letters*, 48(20), e2021GL094289. <https://doi.org/10.1029/2021gl094289>
- Roth, L., Alday, J., Becker, T. M., Ivchenko, N., & Retherford, K. D. (2017a). Detection of a hydrogen corona at Callisto. *Journal of Geophysical Research: Planets*, 122(5), 1046–1055. <https://doi.org/10.1002/2017je005294>
- Roth, L., Ivchenko, N., Gladstone, G. R., Saur, J., Grodent, D., Bonfond, B., et al. (2021). A sublimated water atmosphere on Ganymede detected from Hubble Space Telescope observations. *Nature Astronomy*, 5(10), 1043–1051. <https://doi.org/10.1038/s41550-021-01426-9>
- Roth, L., Retherford, K. D., Ivchenko, N., Schlatter, N., Strobel, D. F., Becker, T. M., & Grava, C. (2017b). Detection of a hydrogen corona in HST Ly $\alpha$  images of Europa in transit of Jupiter. *The Astronomical Journal*, 153(2), 67. <https://doi.org/10.3847/1538-3881/153/2/67>
- Roth, L., Saur, J., Retherford, K. D., Strobel, D. F., Feldman, P. D., McGrath, M. A., et al. (2016). Europa's far ultraviolet oxygen aurora from a comprehensive set of HST observations. *Journal of Geophysical Research: Space Physics*, 121(3), 2143–2170. <https://doi.org/10.1002/2015ja022073>
- Saur, J., Feldman, P. D., Roth, L., Nimmo, F., Strobel, D. F., Retherford, K. D., et al. (2011). Hubble space telescope/advanced camera for surveys observations of Europa's atmospheric ultraviolet emission at eastern elongation. *The Astrophysical Journal*, 738(2), 153. <https://doi.org/10.1088/0004-637x/738/2/153>
- Saur, J., Strobel, D. F., & Neubauer, F. M. (1998). Interaction of the jovian magnetosphere with Europa: Constraints on the neutral atmosphere. *Journal of Geophysical Research*, 103(E9), 19947–19962. <https://doi.org/10.1029/97je03556>
- Schafer, D., Newman, J., Smith, K., & Stebbings, R. (1987). Differential cross sections for scattering of 0.5-, 1.5-, and 5.0-keV oxygen atoms by He, N<sub>2</sub>, and O<sub>2</sub>. *Journal of Geophysical Research*, 92(A6), 6107–6113. <https://doi.org/10.1029/ja092ia06p06107>
- Shematovich, V. I. (2006). Stochastic models of hot planetary and satellite coronas: Atomic oxygen in Europa's corona. *Solar System Research*, 40(3), 175–190. <https://doi.org/10.1134/s0038094606030014>
- Shematovich, V. I., & Johnson, R. E. (2001). Near-surface oxygen atmosphere at Europa. *Advances in Space Research*, 27(11), 1881–1888. [https://doi.org/10.1016/s0273-1177\(01\)00299-x](https://doi.org/10.1016/s0273-1177(01)00299-x)
- Shematovich, V. I., Johnson, R. E., Cooper, J. F., & Wong, M. C. (2005). Surface-bounded atmosphere of Europa. *Icarus*, 173(2), 480–498. <https://doi.org/10.1016/j.icarus.2004.08.013>
- Smith, H. T., Mitchell, D. G., Johnson, R. E., Mauk, B. H., & Smith, J. E. (2019). Europa neutral torus confirmation and characterization based on observations and modeling. *The Astrophysical Journal*, 871(1), 69. <https://doi.org/10.3847/1538-4357/aaed38>
- Smyth, W. H., & Marconi, M. L. (2006). Europa's atmosphere, gas tori, and magnetospheric implications. *Icarus*, 181(2), 510–526. <https://doi.org/10.1016/j.icarus.2005.10.019>
- Szalay, J. R., Allegrini, F., Ebert, R. W., Bagenal, F., Bolton, S. J., Fatemi, S., et al. (2024). Oxygen production from dissociation of Europa's water-ice surface. *Nature Astronomy*, 8(5), 567–576. <https://doi.org/10.1038/s41550-024-02206-x>
- Szalay, J. R., Smith, H. T., Zirnstein, E. J., McComas, D. J., Begley, L. J., Bagenal, F., et al. (2022). Water-group pickup ions from Europa-genic neutrals orbiting Jupiter. *Geophysical Research Letters*, 49(9), page e2022GL098111. <https://doi.org/10.1029/2022gl098111>
- Teolis, B. D., Wyrick, D. Y., Bouquet, A., Magee, B. A., & Waite, J. H. (2017). Plume and surface feature structure and compositional effects on Europa's global exosphere: Preliminary Europa mission predictions. *Icarus*, 284, 18–29. <https://doi.org/10.1016/j.icarus.2016.10.027>
- Turc, L., Leclercq, L., Leblanc, F., Modolo, R., & Chaufray, J.-Y. (2014). Modelling Ganymede's neutral environment: A 3D test-particle simulation. *Icarus*, 229, 157–169. <https://doi.org/10.1016/j.icarus.2013.11.005>
- Vorbürger, A., Fatemi, S., Galli, A., Liuzzo, L., Poppe, A. R., & Wurz, P. (2022). 3D Monte-Carlo simulation of Ganymede's water exosphere. *Icarus*, 375, 114810. <https://doi.org/10.1016/j.icarus.2021.114810>
- Vorbürger, A., Fatemi, S., Mogan, S. R. C., Galli, A., Liuzzo, L., Poppe, A. R., et al. (2024). 3D Monte-Carlo simulation of Ganymede's atmosphere. *Icarus*, 409, 115847. <https://doi.org/10.1016/j.icarus.2023.115847>
- Vorbürger, A., & Wurz, P. (2018). Europa's ice-related atmosphere: The sputter contribution. *Icarus*, 311, 135–145. <https://doi.org/10.1016/j.icarus.2018.03.022>
- Waite, J. H., Jr., Greathouse, T. K., Carberry Mogan, S. R., Sulaiman, A. H., Valek, P., Allegrini, F., et al. (2024). Magnetospheric-ionospheric-atmospheric implications from the Juno flyby of Ganymede. *Journal of Geophysical Research: Planets*, 129(4), e2023JE007859. <https://doi.org/10.1029/2023je007859>

### References From the Supporting Information

- Brinkmann, R. T. (1970). Departures from Jeans' escape rate for H and He in the Earth's atmosphere. *Planetary and Space Science*, *18*(4), 449–478. [https://doi.org/10.1016/0032-0633\(70\)90124-8](https://doi.org/10.1016/0032-0633(70)90124-8)
- Huebner, W. F., & Mukherjee, J. (2015). Photoionization and photodissociation rates in solar and blackbody radiation fields. *Planetary and Space Science*, *106*, 11–45. <https://doi.org/10.1016/j.pss.2014.11.022>
- Johnson, R. E., Boring, J. W., Reimann, C. T., Barton, L. A., Sieveka, E. M., Garrett, J. W., et al. (1983). Plasma ion-induced molecular ejection on the Galilean satellites: Energies of ejected molecules. *Geophysical Research Letters*, *10*(9), 892–895. <https://doi.org/10.1029/g1010i009p00892>
- Smith, G. R., Shemansky, D. E., Broadfoot, A. L., & Wallace, L. (1978). Monte Carlo modeling of exospheric bodies: Mercury. *Journal of Geophysical Research*, *83*(A8), 3783–3790. <https://doi.org/10.1029/ja083ia08p03783>
- Spencer, J. R., Tamppari, L. K., Martin, T. Z., & Travis, L. D. (1999). Temperatures on Europa from galileo photopolarimeter-radiometer: Nighttime thermal anomalies. *Science*, *284*(5419), 1514–1516. <https://doi.org/10.1126/science.284.5419.1514>